Chalcogenide Letters Vol. 16, No. 6, June 2019, p. 257 – 263

# EFFECT OF INSERTION OF ALUMINUM NANOSHEETS ON THE STRUCTURAL, OPTICAL AND DIELECTRIC PROPERTIES OF STACKED LAYERS OF SELENIUM

A. F. QASRAWI[a,b], O. H. ABU AL ROB[a]
[a]*Department of Physics, Arab-American University, Jenin, Palestine*
[b]*Group of Physics, Faculty of Engineering, Atilim University, 06836 Ankara, Turkey*

In this work, the time dependent metal induced crystallization process in stacked layers of selenium that are sandwiched with aluminum nanosheets of thicknesses of 50 nm are investigated by means of X-ray diffraction and optical spectrophotometry techniques. The Al nanosheets motivated the growth of orthorhombic phases of selenium and lowered the energy bang gap of the amorphous films from 2.26 to 1.82 eV when the orthorhombic phase is achieved. The time dependent monitoring of the structural and optical properties over eighteen months have shown that both of the orthorhombic and amorphous phases exhibit a second transformation to hexagonal and stabilize at that phase within ten days of the growth time. The presence of the aluminum nanosheets enhanced the light absorbability by 15 and 5 times in the orthorhombic and hexagonal phases, respectively. In addition, the dielectric spectra of the studied films display similar characteristics in the hexagonal phase with slight differences that results from Al nanosheets. The dielectric spectra for both of the amorphous and orthorhombic phases displayed resonance peaks in the visible and infrared ranges of light. The structural and optical analysis that are carried out through this study represent a guide for using the selenium films in optoelectronic technology.

(Received March 5, 2019; Accepted Accepted June 1, 2019)

*Keywords*: Amorphous selenium, Orthorhombic-hexagonal, Optical properties, Metal-semiconductor interface

## 1. Introduction

Selenium thin films have been under the focus of research centers since decades owing to its wide range of applications. They have been used for fabrication of thin film transistors and photonic devices [1].Selenium is also used for the production of optoelectronic devices like solar cells [2]. Amorphous selenium solar cells are reported to reveal a short circuit current and an open circuit voltage of 10.2 mA/cm$^2$, 0.911 V, respectively. The filling factor and efficiency of these cells reached 55% and 5.2%, respectively [2]. In addition, Se is also regarded as promising material for use in optical fibers [3]. Literature data reported the possibility of fabrication of optical fiber with a diameter of 0.22 mm from Se glasses containing 20% germanium ($Ge_{20}Se_{80}$). The optical loss of this fiber in the spectral range of 5-8 $\mu m$ is at the level of 1.2-1.6 dB/m.

Interfacing of Se with metals and/or using it as substrate for semiconducting materials is reported to enhance the performance of optoelectronic devices and of electronic circuit components. As for example, Al-Se which is used as rechargeable batteries [4] are found to able to deliver a high reversible capacity of 178 mAh g$^{-1}$ with high discharge voltages mainly above 1.5 V. In addition, Se substrates are considered as promising layers to enhance the efficiency of $Cu_2ZnSn(S_xSe_{1-x})_4$ tandem solar cells [5]. The use of Se raises the efficiency of these cells to ~30% which is a very high percentage in the word of solar cells.

The above mentioned applications of Se and the features of the selenium as substrate motivated us to explore the effects of insertion of metal nanosheets between layers of Se in an

*Corresponding author: atef.qasrawi@atilim.edu.tr

attempt to enhance their optical performance. Thus, here in this work, aluminum nanosheets of thicknesses of 50 nm are inserted between two layers of selenium by the thermal evaporation method under high vacuum pressure. The produced films are structurally and optically characterized in two stages. One within the first day of production and the other as time passes. Trails are tested each six month to observe the stability of the produced films.

## 2. Experimental details

High purity (99.99%) selenium grains are used as source material to produce Se thin films. For this purpose VCM-600 thermal vacuum evaporator is used to prepare the films onto ultrasonically cleaned glass substrates. After situating the Se grains in a tungsten boat, the vacuum pressure was kept at $10^{-5}$ mbar before the evaporation starts. The thickness of the Selenium layer was recorded via INFICON- STM2 thickness monitor that can carry 3000 reading per second and has resolution of 0.03 Å. Each stacked layer of Se was 400 nm thick. To insert Al nanosheets, the first layer of Se was grown and then used as substrate to grow 50 nm Al (99.999%). The Se/Al films are kept in the system till another 400 nm thick layer of Se is re-deposited onto the grown glass/Se/Al layers. The structural characterizations are carried out with the help of Miniflex 600 X-ray diffraction unit (10-70$^o$ at a scanning speed of 1$^o$/min). The optical transmittance and reflectance were measured using thermos-scientific Evolution 300 spectrophotometer equipped with VEE MAX II reflectometer.

## 3. Results and discussion

The X-ray diffraction patterns for the freshly produced Se/Se (SAlS-0) )and Se/Se sandwiched with 50 nm thick Aluminum (SAlS-50) thin films are shown in inset-1 of Fig.1. Owing to the appearance of no intensive peaks, it is clear from the inset of the figure that the fresh Se/Se films exhibit amorphous nature of structure. Insertion of 50 nm Al nanosheet between layers of Se motivated he crystallization process in Se. The analysis of the observed sharp patterns with the help of "Crystdiff" software packages indicated the formation of the orthorhombic phase of Se. The most intensive peak is oriented in the (100) direction. The Miller indices ($hkl$) which appear in inset-1 are assigned using the lattice parameters, $a = 3.201, b = 4.098, c = 3.660$ Å [6] of the orthorhombic phase with the help of the equation, $d_{hkl}^{-2} = \frac{h^2}{a^2} + \frac{k^2}{b^2} + \frac{l^2}{c^2}$. The crystallization process in selenium is induced by Al nanosheets. Aluminum is known to induce the crystallization of many materials like silicon [7] and Ge thin films [8]. The induction of crystallization by the presence of Al was previously assigned to the diffusion of Al atoms into the structure of Ge [8]. For our case, as the bond length of Al-Al being 2.45 A [9] is longer than that of Al-Se (2.35 A [10]), weak bonds and broken bonds of Al at the interface would prefer formation of $Al_2Se_3$ at the interface due to the stronger Coulombic interaction between Se and Al. Al insertion between layers of ZnSe was also observed to strongly affect the crystallinity of ZnSe [10]. It caused lattice contraction which results in strain and stress that provides extra internal energy on the randomly distributed Se rings forcing then to exhibit regular arrays. The same behavior was also reported for amorphous Ge coated onto Al substrate [8]. Diffusion of Al forced formation of AlGe clusters.

When the experiments were repeated three weeks later, an interesting feature was detected for the SAS-0 and SAS-50 films. Namely, as appears in Fig. 1, the pure selenium film crystallize with time showing hexagonal nature of structure and the orthorhombic phase of Se/Al/Se films relax to hexagonal structure. Daily detection of the crystallization process has shown that the crystalline phase appears ten days since the time of growth. The hexagonal planes which represent most of the structure are best oriented in the (010) direction. The final stabilized structure of Se thin films was re-evaluated six months, one year and one and half year latter. No change in the crystalline nature was observed. It means that the stacked layers of Se and Al sandwiched Se prefers the hexagonal nature of structure over that of orthorhombic. As Fig. 1 also demonstrates the orthorhombic phase still exist as minor phase in the structure of Se. The main difference

between these two structural phases is in the molecular ring shapes. Particularly, while the orthorhombic selenium is formed from $Se_7$ ring molecules, $Se_6$ results in the formation of hexagonal selenium, [11]. The orthorhombic $Se_7$ molecule is formed from chair -type and boat-ring types. It is reported that, for tetragonal and monoclinic Se, the bond angles are 103.7°, 105.3°, respectively [11]. While for the rhombohedral (hexagonal) structure the dihedral angle is 76°, the orthorhombic chair types exhibit flexible dihedral angles that can take any value in the range of 0-113°. In the light of these information it is possible to think that the chair like $Se_7$ rings exhibit slow time dependent reaction which results in losing one Se atom leading to the formation of $Se_6$ rings that in turn prefer the hexagonal phase of formation.

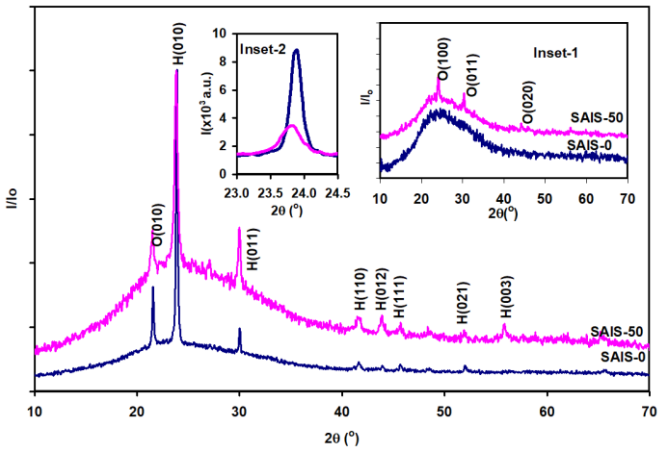


*Fig. 1. The X-ray diffraction patterns for Se/Se and Se/Al/Se films after achieving structural stability Inset-1 show the XRD patterns of the freshly produced films. Inset-2 shows the Al nanosheets effect on the main reflection peak.*

Inset-2 of Fig. 1 displays the effect of Al nanosheets on the main peak of the hexagonal structure. It is evident from the inset of figure that the insertion of Al leads to a sharp decrease in the XRD intensity and causes broadening and shift in the peaks positions. Namely, the peaks which appear at diffraction angles of $2\theta = 23.90^{o}$ with intensity value of 8440 counts/s shifts to $2\theta = 23.80^{o}$ and exhibit maximum intensity values of 3440 counts/s. The lower the X-ray diffraction intensity, the less the number of oriented planes along a specific direction. The calculated lattice parameters ($a$=3.721, $c$=4.939 Å), crystallite size ($D = 42$ nm), microstrain ($\epsilon = 4.12 \times 10^{-3}$) and defect density ($\delta = 3.92 \times 10^{11}\ lines/cm^2$) in accordance with the previously reported equations [12] from the maximum peak broadening and position have shown that, the lattice constants increase along the $a$-axis to $a$=3.736 and decreases along the $c$-axis to $c$=4.925 Å upon insertion of Al nanosheet between layers of Se. In addition, while the microstrain and defect density increases exhibiting values of $6.21 \times 10^{-3}$ and $8.82 \times 10^{11}\ lines/cm^2$, respectively, the crystallite sizes decreases to 28 nm as a result of Al sandwiching between layers of Se. Since the strain and stress are directly related, then, the results assure that the structural modifications have resulted from the strain and stress that increased the internal energy of the system leading to the observed deformation effects. Similar behavior was also observed for indium sandwiched ZnSe thin films [12].

The effects of crystallization and phase type on the optical properties of Se/Se and Se/Al/Se films are investigated by means of visible light spectrophotometry technique. The absorption coefficient ($\alpha$) spectra which are calculated from the measured transmittance and reflectance spectra in accordance with the previously reported equations [12] is shown in Fig. 2. While Fig. 2 (a) illustrates the absorption coefficient spectra for the freshly measured films which reveal amorphous nature of structure for the Se/Se stacked layers and orthorhombic phase for the Se/Al/Se films, Fig. 2 (b) illustrate the absorption coefficient measured at late time (each six

months) where the phase transitions stabilize as hexagonal structure for both of the SALS-0 and SALS-50 samples. As seen from Fig. 2 (a) and (b), the presence of Al nanosheets in the samples increases the value of the absorption coefficient and causes a redshift in the spectra. The ratio of the absorption coefficients before and after the insertion of Al nanosheets ($R_\lambda = \frac{\alpha_{SAlS-50}}{\alpha_{SAlS-0}}$) which is illustrated in the insets of the figures indicates that a significant enhancement in the light absorbability is achieved via Al participation in the structure of Se. Two maxima are observed in $R_\lambda$ spectra (inset of Fig. 2(a)) of the freshly prepared films one is at 1.94 eV and the other is at 1.17 eV. The material becomes highly sensitive to visible and infrared light spectrum upon insertion of Al nanosheets. Al improved the light absorbability by 15 times in the IR region. In addition, for the same samples which exhibit hexagonal structure after it becomes structurally stable, $R_\lambda$ spectra increases with decreasing incident photon energy reaching a value of 5.07 at 1.26 eV. Again the light absorbability of Se is enhanced by the insertion of Al in its structure. However, the structural transformations from orthorhombic to hexagonal significantly reduces the light absorbability by three times. It is also readable from Fig. 2 (a) and (b) that the insertion of Al nanosheets forced the material to exhibit nonzero $\alpha$ values even at very low incident photon energy. Such behavior means the formation of band tails or interbands in the energy band gap of the Se [13]. Interbands may have resulted from the defects which are observed to increase via Al participation in the structure of Se.

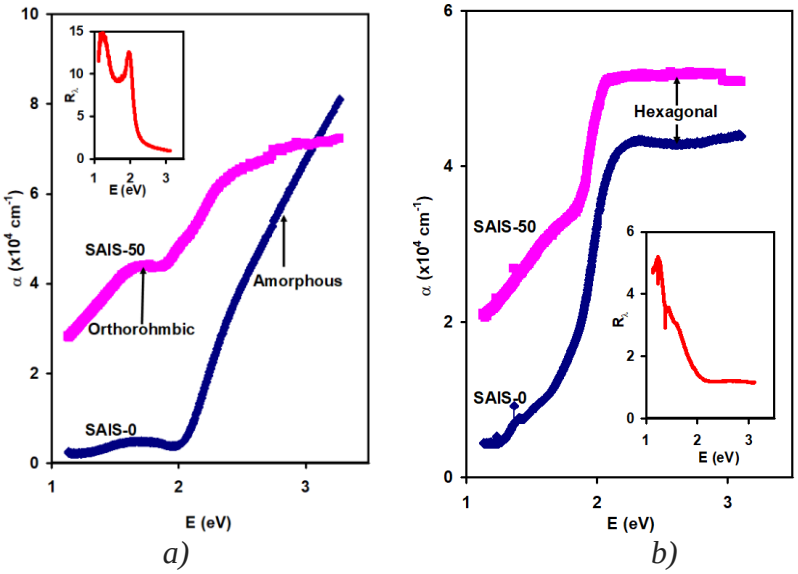


*Fig. 2. The absorption coefficient spectra of Se/Se and Se/Al/Se stacked layers for (a) the freshly produced and (b) for the films after achieving structural stability. Insets of (a) and of (b) show the respective light absorbability.*

The effects of the structural transformations and Al nanosheets insertion on the optical energy band gap of stacked layers of Se is determined from the Tauc's equation ($(\alpha E)^2 \propto (E - E_g)$ [12]) plotting's which exhibit in the $E$-axis crossings that are displayed in Fig. 3 (a) and (b). The $E-$axis crossing's reveals direct allowed energy band gap values of 2.26 eV for the amorphous SAlS-0 films, 1.82 eV for orthorhombic SAlS-50 films, 1.86 eV for hexagonal SAlS-0 and 1.79 eV for SAlS-50 films. The Al-induced crystallization process in Se films is accompanied with large redshift in the energy band gap. The energy band gap difference is $\Delta E_g = 0.44\ eV$. In addition, the structural transformation from amorphous to hexagonal in SAlS-0 films leads to energy band gap difference of $\Delta E_g = 0.40\ eV$. The Al decreased the band gap of the hexagonal phase by 0.07 eV. Except for the induced crystallization process, Al insertion between two layers of Se does not significantly alter the band gap but enhanced the light absorbability as we mentioned before. The reason for the large shift in the value of the energy band gap upon

structural transformation is the exchange in shape of the Se rings. The energy band gap values mentioned here are consistent with literature data [14] which reports value of 2.15 eV for amorphous Se and 1.80 eV for hexagonal Se [15]. In accordance with the density of state calculations [16] which take into account the orbital –projections in Se, the lowest valence bands that extend from -15.9 to -9.5 eV originate from the *s* orbitals. The top valence bands that lay in the range from -5.9 to 0.0 eV and the lower conduction bands that exist in the range from 1.0 to 4.0 eV originates primarily from the $p$ orbitals. Considering the degeneracy of the $p$ states, the lower valence bands ( from -5.9 to -4.2 eV) and the lower conduction bands (from 1.9 to 3.3 eV ) are established by the $p_z$ orbital with some contributions from the $p_x$ and $p_y$ orbitals [16]. On the other hand, valence bands maxima which extends from -4.2 to 0.0 eV are mainly assigned to $p_x$ and $p_y$ orbitals with some contribution of $p_z$ component. Furthermore, the absolute minima of conduction bands are found to be distributed in the range of 1.2- 1.9 eV and originates mainly from $p_y$ orbitals. As the structural modifications are accompanied with exchanges in the Se rings from $Se_7$ to $Se_6$ and as the amorphous Se may comprise $Se_6$, $Se_7$ and $Se_8$ molecular rings in its structure, the density of the orbitals changes accordingly. Particularly, the orthorhombic phase mostly composed of $Se_7$ rings which exhibit different density of orbitals due to the lack of $Se_8$ molecular rings (present in amorphous ) and this could be main reason for the significant narrowing in the energy band gap of Se [6, 11].

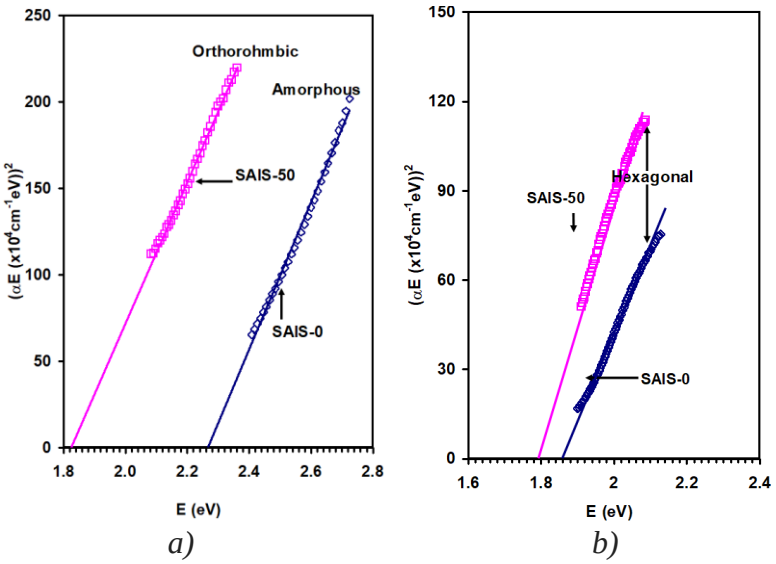


*Fig. 3. (a) The Tauc's equation fittings for the (a) freshly produced and (b) stable Se/Se and Se/Al/Se films.*

Fig. 4 (a) and (b) display the real part of the dielectric spectra ($\varepsilon_r$) for the samples under study as calculated from the measured transmittance and reflectance with the help of Fresnel's equation for light at normal incidence [10, 17]. For amorphous Se, $\varepsilon_r$ spectra exhibit a peak centered at 1.71 eV with maximum dielectric constants value of 10.32. When the material change structure to orthorhombic phases which is achieved via Al nanosheet insertion, the shape of the dielectric spectra completely change and two broadened peaks with values of 8.22 and 8.53 are observed at 1.69 and at 1.30 eV, respectively. The high frequency dielectric constant ($\varepsilon_\infty$) significantly decreased from 5.33 to 2.96 as the material changes structure from amorphous to orthorhombic phases. The dielectric spectra of the hexagonal phase which is shown in Fig. 4 (b) display no significant effect of Al on the values of $\varepsilon_\infty$. The dielectric spectra of the hexagonal phases display peaks at 1.44 and 1.28 eV for the SAlS-0 sample and at 1.19 eV for the SAlS-50 sample. While transitions from $p_x$ at 0.0 eV to $p_y$ orbitals at 1.90 eV could account for the observed peak at 1.71 and at 1.69 eV, transitions from the top of the valence band in $p_x$ state at

0.0 eV to the absolute minima of the conduction band at 1.20 eV of the $p_y$ state could account for the observed peaks near 1.44 and 1.30 eV. The addition of Al nanosheets and their interaction with Se atoms at the interface brings to mind the attenuations that arises from the changes in the electronic configurations. Al has the electronic configuration of $3s^2 3p^1$ which is at lower energy levels than that of Se which has the $4s^2 4p^4$. Interaction between Al and Se to form $Al_2Se_3$ provide one extra unbonded valence electron from Al that increases the number of free electrons in Se which in turn reduces the value of the real part of the dielectric constant owing to the availability of much free carriers [18]. Alternatively, as the Al provides three valence electrons on the metal surface, the interfacing with $p$ −type Se whose work function is 5.11 eV which is larger than the work function of Al (4.24 eV) [19] leads to Schottky nature of contact. In this type of contacts holes flow from Se to Al to reach equilibrium at the Fermi surface. As the Al is at midpoint between the two layers of Se, identical loss in the number of holes is expected. However, band bending at both sides still possible. The band bending which leads the reduction of the electric field in bulk of the samples could account for the reduction in the values of the high frequency dielectric constant [20].

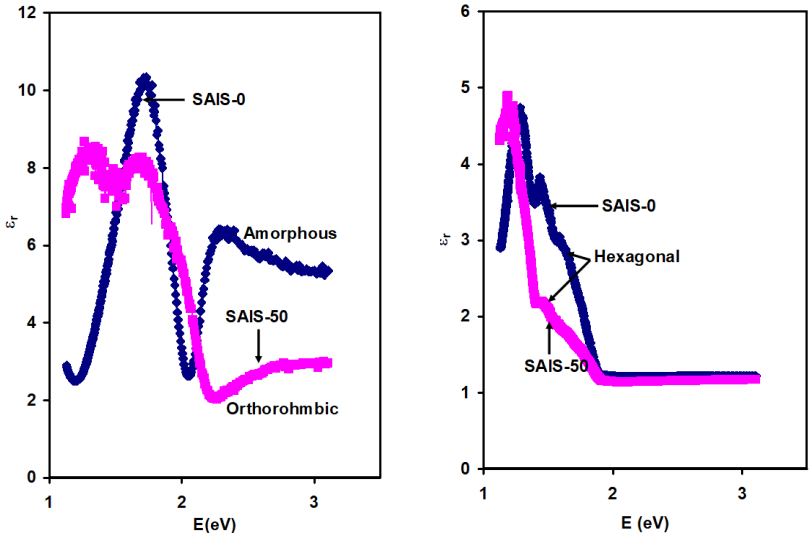


*Fig. 4. The real part of the dielectric spectra for the (a) freshly produced and (b) stable Se/Se and Se/Al/Se films.*

## 4. Conclusions

In this work, we have explored the effects of aluminum nanosheets insertion of the structural and optical properties of two stacked layers of selenium. While the presence of Al between layers of selenium induced the growth of orthorhombic phases of Se, the time dependent studies has shown that the films exhibit phase transitions from amorphous and from orthorhombic to hexagonal structure. The metal induced and time dependent crystallization processes strongly affected the electrical and dielectric properties of the films.

A significant shrinkage in the energy band gap by 0.44 eV is detected upon amorphous-orthorhombic structural transformations and band gap shrinkage of 0.40 eV is achieved upon amorphous-hexagonal transformations. The presence of Al nanosheets which caused orthorhombic-hexagonal transformations have no significant effect on the value of the energy band gap. In addition, the observed structural transformations highly influenced the dielectric properties of the stacked layers of selenium. The Al nanosheets decreased the values of the dielectric constant and change the shapes of the spectra.

**Acknowledgements**

This project was funded by the Deanship of Scientific Research (DSR) at the Arab American University, Palestine (AAUP). The authors, therefore, acknowledge with thanks the DSR and the AAUP technical and financial support for the 2018-2019 Cycle I project.

## References

[1] W. Yan, A. Burgos-Caminal, T. D. Gupta, J. –E. Moser, F. Sorin, The Journal of Physical Chemistry C **122**(43), 25134 (2018).
[2] I. Hadar, T.- B. Song, W. Ke, M. G. Kanatzidis, Advanced Energy Materials, 1802766 (2019).
[3] A. P. Velmuzhov, M. V. Sukhanov, V. S. Shiryaev, M. F. Churbanov, T. V. Kotereva, N. S. Zernova, D. A. Fadeeva. Optical Materials **84**, 888 (2018).
[4] X. Huang, Y. Liu, Ch. Liu, J. Zhang, O. Noonan, Ch. Yu, Chemical science **9**(23), 5178 (2018).
[5] H. Ferhati, F. Djeffal, Physica E: Low-dimensional Systems and Nanostructures **109**, 52 (2019).
[6] D. R. McCann, L. Cartz, The J. Chem. Phys. **56**(6), 2552 (1972).
[7] Jr. Hainey, F. Mel, Z. Y. Al Balushi, K. Wang, N. C. Martin, A. Bansal, M. Chubarov, J. M. Redwing, Physica status solidi (RRL)–Rapid Research Letters **12**(3), 1700392 (2018).
[8] F. Katsuki, K. Hanafusa, M. Yonemura, T. Koyama, M. Doi, Journal of Applied Physics **89**(8), 4643 (2001).
[9] X. Zhang, I. A. Popov, K. A. Lundell, H. Wang, Ch. Mu, W. Wang, H. Schnöckel, A. I. Boldyrev, K. H. Bowen, Angewandte Chemie **130**(43), 14256 (2018).
[10] A. F. Qasrawi, A. M. Alsabe, Materials Research Express (2019).
[11] T. Takahashi, Sh. Yagi, T. Sagawa, K. Nagata, Y. Miyamoto, J. Phys. Soc. Japan **54**(3), 1018 (1985).
[12] S. E. Al Garni, A. F. Qasrawi, Results in physics **7**, 4168 (2017).
[13] A. Abouelsayed, B. Anis, A. Okasha, A. M. Ali, W. Elhotaby, A. S. G. Khalil, Materials Chemistry and Physics **203**, 1 (2018).
[14] J. Li, X. Zhu, Q. Xie, G. Pu, D. Yan, Journal of Materials Science: Materials in Electronics **29**(22), 19256 (2018).
[15] M. Zhu, G. Niu, J. Tang, Journal of Materials Chemistry *C* **7**(8), 2199 (2019).
[16] M. Cheng, Sh. Wu, Z. –Z. Zhu, G. –Y. Guo, arXiv preprint arXiv:1904.01927 (2019).
[17] A. F. Qasrawi, M. F. Taleb, Chalcogenide Letters **16**(3), 95 (2019).
[18] M. Fox, Optical properties of solids, 1269 (2002).
[19] S. Alotaibi, K. N. Manjunatha, Sh. Paul, Applied Surface Science **424**, 330 (2017).
[20] P. Servati, A. Nathan, IEEE Transactions on Electron Devices **49**(5), 812 (2002).